Using the Thermal Ratchet Mechanism to Achieve Net Motility in Magnetic Microswimmers

Gouri Patil
Department of Physics, Indian Institute of Science, Bangalore 560012, India

Pranay Mandal
Centre for Nano Science and Engineering, Indian Institute of Science, Bangalore 560012, India

Ambarish Ghosh[*,†]
Centre for Nano Science and Engineering, Indian Institute of Science, Bangalore 560012, India

(Received 10 May 2022; revised 12 September 2022; accepted 7 October 2022; published 31 October 2022)

Thermal ratchets can extract useful work from random fluctuations. This is common in the molecular scale, such as motor proteins, and has also been used to achieve directional transport in microfluidic devices. In this Letter, we use the ratchet principle to induce net motility in an externally powered magnetic colloid, which otherwise shows reciprocal (back and forth) motion. The experimental system is based on ferromagnetic micro helices driven by oscillating magnetic fields, where the reciprocal symmetry is broken through asymmetric actuation timescales. The swimmers show net motility with an enhanced diffusivity, in agreement with the numerical calculations. This new class of microscale, magnetically powered, active colloids can provide a promising experimental platform to simulate diverse active matter phenomena in the natural world.

DOI: 10.1103/PhysRevLett.129.198002

Active matter refers to systems of interacting entities that can convert local energy input into independent displacements and meaningful work [1,2]. Examples include a wide range of length scales and phenomena [3], ranging from molecular motors in intracellular biochemical processes to bacterial colonies and human migration. There have been significant efforts to develop artificial, motile entities that provide test platforms for studying various active matter phenomena. Of special interest are colloidal particles driven by light [4,5], electric [6–8], magnetic [9] field, and chemical [10] reactions, whose activities could be externally controlled while ensuring the energy transduction occurs independently and locally at the scale of individual colloids.

Magnetic powering [11] provides unique advantages in the experimental investigation of nonequilibrium systems, with easy external control over the activity. Previous studies have included dynamic self-organization of magnetic colloids under external drive, which forms fascinating active materials through collective interactions [12–14], or through asymmetric interactions [15] with a surface. The work reported here is fundamentally different, in which we report a magnetically powered active system, where there is motility induced at the scale of a single colloid in a bulk medium, employing ambient thermal fluctuations.

The only magnetically powered active swimmer reported [9,16–18] so far is based on a versatile experimental platform, comprising magnetic, helical nanostructures suspended in a fluid. The colloidal system is stable and maneuverable in most fluids [19–22] and powered by small, spatially homogeneous magnetic fields, with complete control over the various experimental parameters, such as the rheological properties of the surrounding medium [20,23] and the activity. The hydrodynamic flow generated by these swimmers is similar to many living active systems at low Reynolds numbers [24], such as various species of flagellated bacteria. However, these swimmers demonstrate back and forth motion, implying zero net motility and thus classified as "reciprocal" swimmers, following the terminology in [24].

Here, we demonstrate a magnetically powered active particle that shows net displacement over a cycle of the magnetic drive, thus qualifying as a "nonreciprocal" swimmer. Interestingly, the micron-scale swimmers reported here are rendered motile by rectifying ambient thermal fluctuations, akin to the Brownian motors [25–27] commonly encountered at much smaller molecular length scales [28] and different from microscale motion induced by nonequilibrium fluctuations of the surrounding bath [29,30], e.g., in the form of active bacterial suspensions [29,30]. While thermal ratchets are ubiquitous in microfluidic manipulation [31–33], as far as we know, this is the first demonstration of a colloidal particle achieving self-propulsion through the thermal ratchet mechanism.

We used a physical vapor deposition technique called glancing angle deposition (GLAD) [34] to fabricate a

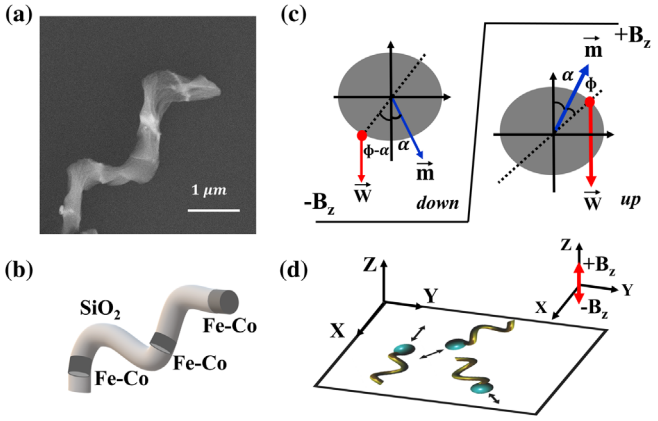

FIG. 1. (a) Scanning electron micrograph and (b) schematic of the microhelix showing the material composition. (c) Schematic of the two possible states of the helix in an oscillating magnetic field. The state ("down") corresponds to the field $-B_z$ has the magnetic moment directed downward, while $+B_z$ corresponds to the "up" state. In the limit of zero thermal noise, the intrinsic mass asymmetry of the helix (shown by $\vec{W}$) caused the down to up transition through a CCW rotation. We do not show the CW rotation from the up to down state, expected when thermal fluctuations are absent. (d) The oscillating field in the z direction results in a reciprocal motion of the swimmers with no constraints on orientation in the XY plane.

helically nanostructured film (see Supplemental Material, Sec. 1 [35]) containing magnetic elements embedded in a dielectric (silica) scaffold. The film is sonicated in water to release individual ferromagnetic micro helices [see Figs. 1(a) and 1(b) for scanning electron micrographs and the schematic] in a microfluidic Hele-Shaw cell. For typical experiments, the helices remain confined in a quasi-2D XY plane, observed under an optical microscope. The helices could be propelled [38] like a corkscrew by applying a spatially uniform rotating magnetic field with speeds proportional to the rotational frequency of the field, provided the driving magnetic torque was more significant than the viscous drag. However, we must stress that this mode of actuation does not qualify [16] the motion to be self-propelled, as the system is subject to a net external torque. As a consequence, the direction of motion for all helices remains identical, defined by the sense of rotation of the field and the handedness of the helix.

The situation changes under a different magnetic drive when the field is oscillated perpendicular [9] to the confining plane, causing the helix to rotate back and forth about its long axis due to an interplay between the magnetic torque and the asymmetric mass distribution of the helices [see Fig. 1(c)]. These clockwise (CW)-counterclockwise (CCW) rotations resulted in the reciprocal linear displacements corresponding to half of their hydrodynamic pitch ($p_H/2$). As shown in Fig. 1(d), the helix directions were independent, qualifying this system of reciprocal swimmers as magnetic active matter. In addition, the thermal noise caused imperfection in the CW-CCW sequence, such as CW-CCW-CW-(CW)-CW-CCW. However, the total number of CW and CCW turns remained the same, resulting in an equal number of forward and backward movements when observed over a long time.

To devise a method to break the reciprocal symmetry of the helical turning sequence and have more CW turns than CCW (or vice versa), we considered the role of thermal noise and actuation timescale $T_{\rm act}$ [see Fig. 1(c)] at which the field is switched from $-B_z$ to $+B_z$. The rotational coordinate α of the helix is governed by two counteracting torques: due to applied magnetic field and mass distribution in the helical structure, as well as intrinsic thermal fluctuations.

$$\gamma_l \frac{d\alpha}{dt} = -mB_z(t)\sin(\alpha) + WR\sin(\alpha+\phi) + \eta_r(t). \quad (1)$$

Here, $\gamma_l \sim 10^{-21}$ kgm^2 s^{-1} is the rotational friction coefficient about the long axis of the swimmer, $m \sim 10^{-16}$ Am^2 is the magnetic moment, $WR \sim 10^{-20}$ N is the torque due to mass asymmetry, and ϕ ($31° \pm 2.7°$) is the angle between the direction of magnetic moment and the line of action of weight (see Supplemental Material, Sec. 2 [35]). The uncorrelated noise is given by $\eta_r(t)$ with $\langle \eta_r(t)\eta_r(t')\rangle = (2k_BT/\gamma_l)\delta(t-t')$, where k_B and T correspond to the Boltzmann constant and ambient temperature, respectively. The form of $B_z(t)$ is shown in Fig. 1(c) with a characteristic actuating time, $T_{\rm act}$. We next rewrite Eq. (1), in terms of $T_W = \gamma_l/WR$ and $T_B = \gamma_l/mB$; timescales related to weight and magnetic torque, respectively:

$$\frac{d\alpha}{dt} = \frac{\sin(\alpha)\cos(\phi)}{T_W} + \frac{\cos(\alpha)\sin(\phi)}{T_W} - \frac{\sin(\alpha)}{T_B} + \eta_r(t). \quad (2)$$

We perform a numerical calculation of the sequence ($-B_z \rightarrow +B_z$) shown in Fig. 1(c), which is expected to be CCW in the absence of thermal fluctuations. We plot the probability of the anomalous CW turn as a function of the actuation timescale in Figs. 2(a) and 2(b), at $\phi = 31°$, for different values of T_B and T_W. The choice of T_B, T_W is based on the experimental system (see Supplemental Material, Sec. 3). Specifically, the curves shown in blue in Fig. 2 represent the timescales of our experiment closely, given by $T_B = 1.5$ and $T_W = 150$ ms. All calculations assumed the ambient temperature to be 300 K. As expected, at lower thermal noise with assumed ambient temperature at 30 K, there are fewer anomalous turns (here, CW). Shorter $T_{\rm act}$ implies a greater number of anomalous turns, with a maximum being 0.5, implying an equal number of CW and CCW turns.

The simulation results and the role of T_B, T_W can be understood by considering the energy diagram of the helix

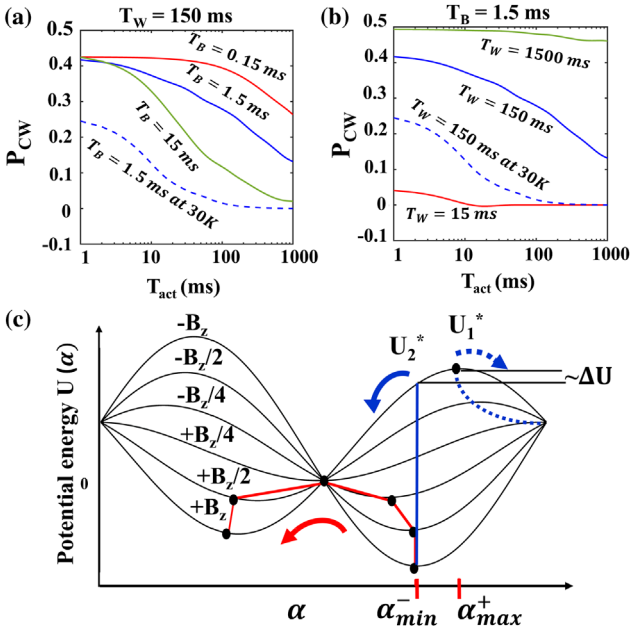

FIG. 2. Following the actuation scheme from $-B_z$ to $+B_z$ shown in Fig. 1(c), calculated probability of an anomalous (here, CW) turn as a function of (actuation time) T_{act}, for different values of (A) T_B and (B) T_W. Also shown is the effect of thermal noise (temperature) in the same graph. (C) The potential energy of the microhelix as a function of α, where red and blue lines show possible paths in configuration space (α) taken by the helix. Solid (red and blue) paths correspond to normal (zero thermal fluctuations) turning events, while anomalous events (dotted blue path) can occur at finite temperatures and at low values of T_{act}.

as a function of α, as shown in Fig. 2(c), and noting its equivalence to the Brownian ratchet [28] potentials. The potential energy is given by

$$U(\alpha) = -mB_z\cos(\alpha) + WR[1+\cos(\alpha+\phi)]. \quad (3)$$

This is in the form of an additive-multiplicative ratchet potential $U(\alpha) = v(\alpha) + f(t)w(\alpha)$, and as far as we know, the general analytical solutions to this problem are not known [39]. As shown in Fig. 2(c), higher T_{act} to go from $-B_z$ to $+B_z$ corresponds to the red path in the configuration space, where the system is always at minimum energy configuration. A faster T_{act} implies a nonequilibrium configuration and two possible paths (shown in blue). In the absence of thermal fluctuations, the swimmers take the solid path ($P_{\mathrm{CW}} = 0$), while the dashed path can occur due to thermal fluctuations, with a probability that depends exponentially on the magnitude of $\Delta U/k_{BT}$, which in turn depends on the experimental system (ϕ, T_B, T_W: see Supplemental Material, Sec. 3 [35]). At higher thermal noise or low T_{act}, the probabilities of the two paths are equal, implying $P_{\mathrm{CW}} = P_{\mathrm{CCW}} = 0.5$. The physical significance of T_{act} can be understood by comparing with the typical experimental timescales T_W and T_B, which are

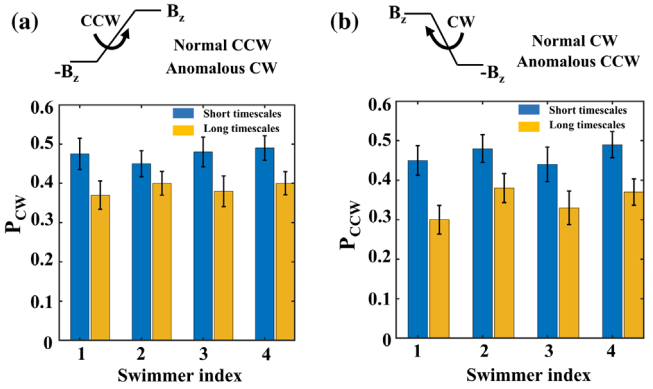

FIG. 3. (a) When B_z goes from -1 to $+1$ mT, there are more CW turns compared to CCW turns when the timescale is shorter (blue bars). (b) Conversely, when B_z goes from $+$B to $-$B, there are more CCW turns compared to CW turns when the timescale is shorter (blue bars).

typically far separated, such that $T_W \gg T_B$. The probability of anomalous turns increases when the actuation timescale T_{act} is closer to and smaller than T_B, i.e., $T_{\mathrm{act}} \leq T_B$, corresponding to the fast actuation timescale [e.g., see green curve shown in Fig. 2(a)]. The probability of anomalous turns decreases when T_{act} is slower, i.e., closer to T_W [e.g., see the solid blue line in Fig. 2(b)]. In summary, slow actuation timescale refers to the case $T_{\mathrm{act}} \geq T_W$. The role of thermal noise can also be understood through a fluctuation timescale, defined as $T_{\mathrm{thermal}} = \gamma/k_BT$. For constant T_W and T_B, the probability of anomalous turns increases when the system is actuated faster than the time in which α randomizes, corresponding to $T_{\mathrm{act}} \leq T_{\mathrm{thermal}}$. The trend becomes opposite with fewer anomalous turns when T_{act} is larger than T_{thermal}. This can be seen in Fig. 3 of the Supplemental Material [35], where the probability of anomalous turns (here CW) is plotted as a function of T_{act}, for different values of thermal noise timescale, T_{thermal}.

The dependence on T_{act} is further confirmed by experiments, where we observe the rotational dynamics of the helix under magnetic actuation at short (10–50 ms) and long (200–1000 ms) actuation timescales. Measurements over various swimmers confirm the increased number of anomalous turns at shorter timescales. These experiments required direct visualization of the turning mechanism, so we used a slightly larger helical nanostructure where it was possible to identify the turning direction easily (see Supplemental Material, Sec. 8 [35]). The graph in Fig. 3 shows the measured probability of anomalous turnings as a function of the magnitude of actuation time (T_{act}), with data from four different swimmers. In Fig. 3(a), when the magnetic field switches from -1 to $+1$ mT, the probability of anomalous (here, CW) turns increases at shorter actuation timescales, which remains consistent across four different swimmers. Similarly, when the field switches from $+1$ to -1 mT, the converse (more CCW turns) occurs, as shown in Fig. 3(b). An essential and difficult

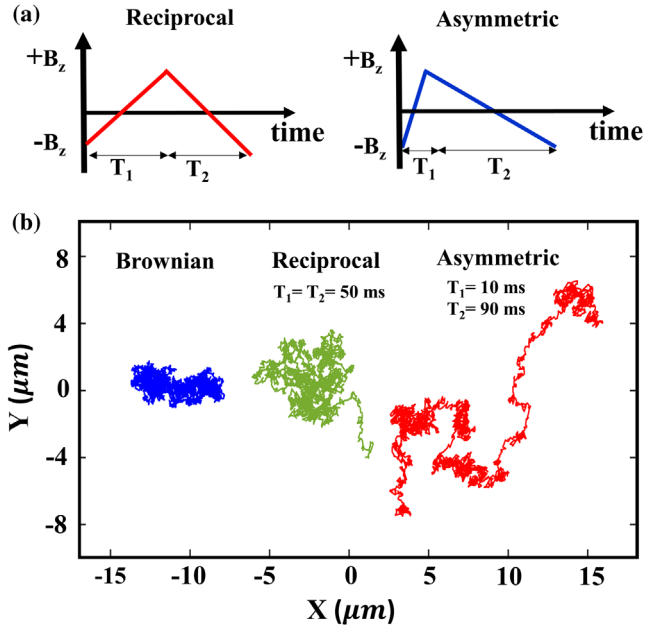

FIG. 4. (a) Schematic of the magnetic actuation drive to break reciprocal symmetry. Timescales $T_1 = T_2$ implies equal number of CW turns, while $T_2 > T_1$ suggests more anomalous CW turns during the $-B_z \rightarrow +B_z$ event, and thus having more CW turns overall. (b) Trajectories acquired over 110 sec for a nonactuated (blue, freely diffusing), reciprocal (green, $T_1 = T_2 = 50$ ms) and two swimmers under asymmetric drive (red, $T_1 = 10$ ms, $T_2 = 90$ ms).

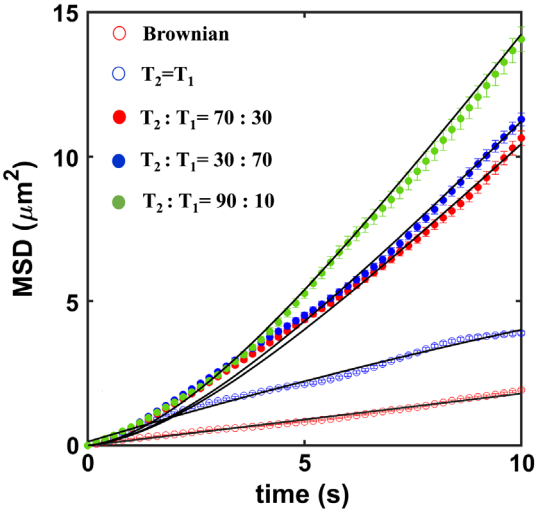

FIG. 5. Mean square displacement (MSD) for a swimmer as a function of time, plotted for different $T_2:T_1$, shows greater diffusivities at higher ratios of $T_2:T_1$. The duration of the actuation cycle $(T_1 + T_2)$ was 100 ms and the curves are fitted with a theoretical fit (see main text). The fit provides effective self-propulsion velocities of 0.54 ± 0.01, 0.45 ± 0.04, 0.47 ± 0.02 μm/s for $T_2:T_1$ ratio varying at 9:1, 7:3, and 3:7, respectively.

aspect of the experiments proposed here is to ensure the field in XY plane is negligibly small; otherwise, it results in alignment and, therefore, the unidirectional motion of the swimmers. This can occur for both dc [40] and ac [41] fields. We use a triaxial Helmholtz coil to circumvent this problem and cancel stray magnetic fields [42] in the XY plane. The correction is further confirmed by checking the orientations of the individual swimmers to be independent at all times. As shown in the Supplemental Material, Sec. 5 [35], we tracked the trajectories of two swimmers under asymmetric drive and subsequently analysed the helix orientations. The orientations were uncorrelated with a correlation coefficient $= 0.0772$. Please note the distance between the swimmers in this experiment was greater than five body lengths, which suggests they were effectively noninteracting.

Having confirmed the dependence of anomalous turns on the actuation timescale, we devise a strategy to break the reciprocal CW-CCW sequence, such as to induce net motion in the helical swimmer. We use an asymmetric magnetic drive, shown schematically in Fig. 4(a). Following the same convention as in Fig. 1(c), we expect a short T_1 resulting in more anomalous events, with maximum being $P_{\mathrm{CW}} = P_{\mathrm{CCW}} = 0.5$. A larger T_2 implies fewer anomalous turns, implying $P_{\mathrm{CW}} > P_{\mathrm{CCW}}$; thus resulting in a greater number of CW turns over a full cycle of magnetic actuation and breaking the reciprocal symmetry. We show the trajectories [see Fig. 4(b)] of a swimmer without magnetic actuation (Brownian motion), reciprocal actuation $(T_1 = T_2)$ and asymmetric drive $(T_2:T_1 \neq 1)$, acquired over approximately 110 sec. The overall increase in the mean squared displacement (asymmetric > reciprocal > Brownian) can be clearly seen.

The increase in diffusivity under reciprocal actuation is well understood [9,43] and related to the orientation fluctuations of the swimmer in the XY plane. However, the diffusivity increased further as the driving field timescales were made asymmetric. This occurred due to an enhanced number of anomalous turns during one cycle of magnetic actuation, resulting in a non-reciprocal stroke pattern, and thus, resulting in a swimmer with net motility. In Fig. 5, we show the mean square displacement for a swimmer (more data for other swimmers available in the Supplemental Material, Sec. 6 [35]) under different levels of actuation asymmetry (given by $T_2:T_1$) and observe the overall diffusivity to indeed increase with higher $T_2:T_1$ values. This easily follows from a larger number of anomalous turns as $T_2:T_1$ increases, as per the numerical simulations shown in Figs. 2(a) and 2(b). The results for $T_2:T_1 = 70$: 30 are similar to $T_2:T_1 = 30$: 70, which implied comparable number of anomalous turns of opposite handedness (CW or CCW) for the two cases.

The linear fit of the MSD with time for Brownian and reciprocal swimmers yield $D_{k_BT} = 5 \times 10^{-14}$ and $D_{\mathrm{reci}} = 1.2 \times 10^{-13}$ m^2 s^{-1}. The increase and oscillatory

dependence of the diffusivity with time for reciprocal actuation was in complete agreement with previous report [9]. The new and interesting aspect of the swimmer under asymmetric actuation was further rise in diffusivity, for which we fit the MSD (for $T_2{:}T_1 = 9$) as per the theoretical description [44,45] for self propelled particles, where MSD $(\tau) = [4D_T + 2v^2\tau_r]\tau + 2v^2\tau_r^2[e^{-\tau/\tau_r} - 1]$, where D_{k_BT} and $\tau_r = 3$ sec (both measured experimentally) corresponds to the Brownian translational and orientational (XY plane) diffusivities of the swimmer. We estimate an effective self propulsion velocity around 0.5 μm/s, which could be increased further by appropriate choice of actuation times. For an actuation cycle with two timescales, fast (shorter) time, T_{fast} and slow (longer) time, T_{slow}, the expected velocity of the swimmer is given by $\{[P_{\text{CW}}(T_{\text{fast}}) - P_{\text{CW}}(T_{\text{slow}})]/[(T_{\text{fast}} + T_{\text{slow}})]\}p_H/2$ where p_H is the hydrodynamic pitch of the swimmer. Considering the fastest actuation time is limited by T_B, i.e., minimum $T_{\text{fast}} = T_B$, we estimated the speed in the present experiment (see Supplemental Material, Fig. 7 [35]) could be as high as 2–3 μm/s. Further increase in speed will be possible by reducing T_B, by either applying higher magnetic fields or using helices with larger magnetic moment [46,47].

In summary, we have realized a new class of active swimmers powered by external magnetic fields. Unlike other synthetic microscale swimmers reported before, the motility of these swimmers is derived from thermal fluctuations using the Brownian ratchet mechanism, which suggests similar strategies may be adopted to develop artificial swimmers at smaller length scales [48]. These self-propelled helical swimmers can be dispersed in various media, including rheologically complex [23] and heterogeneous environments [49], and their motility can be controlled by engineering the magnetic drive. It may be possible to add multiple functionalities to these swimmers, including optofluidic manipulation [50,51]. We believe this experimental system is highly suitable for studying and simulating the various phenomenological models for the wet active matter. It may be particularly interesting to study the interplay of hydrodynamic interactions [52] and noise-induced motility in shaping their collective behavior, as well as individual nonreciprocal dynamics [53] as a function of equilibrium thermal fluctuations. Also, this system is known to be bio-compatible and maneuverable in various biological media [19–21,49,54], implying futuristic biomedical applications emerging from self-propelled, theragnostic [55–58] entities deployed in living systems.

The authors would like to thank Ajay Ajith for his help with the experiments involving cancellation of stray magnetic fields. We gratefully acknowledge DBT, SERB, and MeiTY for funding support, and the usage of the facilities in the Micro and Nano Characterization Facility and National Nano Fabrication Centre (CeNSE) at IISc.

*Also at Department of Physics, Indian Institute of Science, Bangalore 560012, India.
†Corresponding author.
ambarish@iisc.ac.in

[1] S. Ramaswamy, The mechanics and statistics of active matter, Annu. Rev. Condens. Matter Phys. **1**, 323 (2010).
[2] M. C. Marchetti, J.-F. Joanny, S. Ramaswamy, T. B. Liverpool, J. Prost, M. Rao, and R. A. Simha, Hydrodynamics of soft active matter, Rev. Mod. Phys. **85**, 1143 (2013).
[3] C. Bechinger, R. Di Leonardo, H. Löwen, C. Reichhardt, G. Volpe, and G. Volpe, Active particles in complex and crowded environments, Rev. Mod. Phys. **88**, 045006 (2016).
[4] K. Villa and M. Pumera, Fuel-free light-driven micro/nanomachines: Artificial active matter mimicking nature, Chem. Soc. Rev. **48**, 4966 (2019).
[5] F. Kümmel, B. ten Hagen, R. Wittkowski, I. Buttinoni, R. Eichhorn, G. Volpe, H. Löwen, and C. Bechinger, Circular Motion of Asymmetric Self-Propelling Particles, Phys. Rev. Lett. **110**, 198302 (2013).
[6] A. Bricard, J.-B. Caussin, N. Desreumaux, O. Dauchot, and D. Bartolo, Emergence of macroscopic directed motion in populations of motile colloids, Nature (London) **503**, 95 (2013).
[7] J. Yan, M. Han, J. Zhang, C. Xu, E. Luijten, and S. Granick, Reconfiguring active particles by electrostatic imbalance, Nat. Mater. **15**, 1095 (2016).
[8] S. Gangwal, O. J. Cayre, M. Z. Bazant, and O. D. Velev, Induced-Charge Electrophoresis of Metallodielectric Particles, Phys. Rev. Lett. **100**, 058302 (2008).
[9] P. Mandal and A. Ghosh, Observation of Enhanced Diffusivity in Magnetically Powered Reciprocal Swimmers, Phys. Rev. Lett. **111**, 248101 (2013).
[10] W. F. Paxton, S. Sundararajan, T. E. Mallouk, and A. Sen, Chemical locomotion, Angew. Chem., Int. Ed. **45**, 5420 (2006).
[11] R. Dreyfus, J. Baudry, M. L. Roper, M. Fermigier, H. A. Stone, and J. Bibette, Microscopic artificial swimmers, Nature (London) **437**, 862 (2005).
[12] Y. Wang, S. Canic, G. Kokot, A. Snezhko, and I. S. Aranson, Quantifying hydrodynamic collective states of magnetic colloidal spinners and rollers, Phys. Rev. Fluids **4**, 013701 (2019).
[13] K. Han, G. Kokot, O. Tovkach, A. Glatz, I. S. Aranson, and A. Snezhko, Emergence of self-organized multivortex states in flocks of active rollers, Proc. Natl. Acad. Sci. U.S.A. **117**, 9706 (2020).
[14] D. Jin and L. Zhang, Collective behaviors of magnetic active matter: Recent progress toward reconfigurable, adaptive, and multifunctional swarming micro/nanorobots, Acc. Chem. Res. **55**, 2100070 (2021).
[15] A. Kaiser, A. Snezhko, and I. S. Aranson, Flocking ferromagnetic colloids, Sci. Adv. **3**, e1601469 (2017).
[16] P. Mandal, G. Patil, H. Kakoty, and A. Ghosh, Magnetic active matter based on helical propulsion, Acc. Chem. Res. **51**, 2689 (2018).
[17] G. Patil and A. Ghosh, Anomalous behavior of highly active helical swimmers, Front. Phys. **8**, 656 (2021).
[18] P. Fischer and A. Ghosh, Magnetically actuated propulsion at low reynolds numbers: Towards nanoscale control, Nanoscale **3**, 557 (2011).

[19] M. Pal, N. Somalwar, A. Singh, R. Bhat, S. M. Eswarappa, D. K. Saini, and A. Ghosh, Maneuverability of magnetic nanomotors inside living cells, Adv. Mater. **30**, 1800429 (2018).
[20] M. Pal, D. Dasgupta, N. Somalwar, V. Reshma, M. Tiwari, D. Teja, S. M. Narayana, A. Katke, R. Jayshree, R. Bhat *et al.*, Helical nanobots as mechanical probes of intra-and extracellular environments, J. Phys. Condens. Matter **32**, 224001 (2020).
[21] Z. Wu, J. Troll, H.-H. Jeong, Q. Wei, M. Stang, F. Ziemssen, Z. Wang, M. Dong, S. Schnichels, T. Qiu *et al.*, A swarm of slippery micropropellers penetrates the vitreous body of the eye, Sci. Adv. **4**, eaat4388 (2018).
[22] A. Servant, F. Qiu, M. Mazza, K. Kostarelos, and B. J. Nelson, Controlled *in vivo* swimming of a swarm of bacteria-like microrobotic flagella, Adv. Mater. **27**, 2981 (2015).
[23] A. Ghosh, D. Dasgupta, M. Pal, K. I. Morozov, A. M. Leshansky, and A. Ghosh, Helical nanomachines as mobile viscometers, Adv. Funct. Mater. **28**, 1705687 (2018).
[24] E. M. Purcell, Life at low reynolds number, Am. J. Phys. **45**, 3 (1977).
[25] P. Reimann, Brownian motors: Noisy transport far from equilibrium, Phys. Rep. **361**, 57 (2002).
[26] J. Rousselet, L. Salome, A. Ajdari, and J. Prostt, Directional motion of brownian particles induced by a periodic asymmetric potential, Nature (London) **370**, 446 (1994).
[27] R. D. Astumian, Thermodynamics and kinetics of a Brownian motor, Science **276**, 917 (1997).
[28] R. D. Astumian and I. Derényi, Fluctuation driven transport and models of molecular motors and pumps, Eur. Biophys. J. **27**, 474 (1998).
[29] R. Di Leonardo, L. Angelani, D. Dell'Arciprete, G. Ruocco, V. Iebba, S. Schippa, M. P. Conte, F. Mecarini, F. De Angelis, and E. Di Fabrizio, Bacterial ratchet motors, Proc. Natl. Acad. Sci. U.S.A. **107**, 9541 (2010).
[30] N. Koumakis, A. Lepore, C. Maggi, and R. Di Leonardo, Targeted delivery of colloids by swimming bacteria, Nat. Commun. **4**, 2588 (2013).
[31] M. J. Skaug, C. Schwemmer, S. Fringes, C. D. Rawlings, and A. W. Knoll, Nanofluidic rocking brownian motors, Science **359**, 1505 (2018).
[32] L. Bogunovic, R. Eichhorn, J. Regtmeier, D. Anselmetti, and P. Reimann, Particle sorting by a structured microfluidic ratchet device with tunable selectivity: Theory and experiment, Soft Matter **8**, 3900 (2012).
[33] S. Verleger, A. Grimm, C. Kreuter, H. M. Tan, J. A. Van Kan, A. Erbe, E. Scheer, and J. R. van der Maarel, A single-channel microparticle sieve based on Brownian ratchets, Lab Chip **12**, 1238 (2012).
[34] M. M. Hawkeye and M. J. Brett, Glancing angle deposition: Fabrication, properties, and applications of micro-and nanostructured thin films, J. Vacuum Sci. Technol. A **25**, 1317 (2007).
[35] See the Supplemental Material at http://link.aps.org/supplemental/10.1103/PhysRevLett.129.198002 for movies and additional figures and includes Refs. [36,37].
[36] A. Ghosh, D. Paria, H. J. Singh, P. L. Venugopalan, and A. Ghosh, Dynamical configurations and bistability of helical nanostructures under external torque, Phys. Rev. E **86**, 031401 (2012).
[37] L. Zhang, J. J. Abbott, L. Dong, B. E. Kratochvil, D. Bell, and B. J. Nelson, Artificial bacterial flagella: Fabrication and magnetic control, Appl. Phys. Lett. **94**, 064107 (2009).
[38] A. Ghosh and P. Fischer, Controlled propulsion of artificial magnetic nanostructured propellers, Nano Lett. **9**, 2243 (2009).
[39] V. M. Rozenbaum, T. Y. Korochkova, I. V. Shapochkina, and L. I. Trakhtenberg, Exactly solvable model of a slightly fluctuating ratchet, Phys. Rev. E **104**, 014133 (2021).
[40] P. Mandal, V. Chopra, and A. Ghosh, Independent positioning of magnetic nanomotors, ACS Nano **9**, 4717 (2015).
[41] R. B. Leighton and M. Sands, *The Feynman Lectures on Physics* (Addison-Wesley, Boston, MA, USA, 1965), Vol. 2, Chap. 16,17.
[42] G. Patil, P. Mandal, J. Behera, A. Ajith, and A. Ghosh, Cancelling stray magnetic fields to render magnetic nanobots autonomous, in *2022 International Conference on Manipulation, Automation and Robotics at Small Scales (MARSS)* (IEEE, 2022), pp. 1–6.
[43] E. Lauga, Enhanced Diffusion by Reciprocal Swimming, Phys. Rev. Lett. **106**, 178101 (2011).
[44] J. R. Howse, R. A. L. Jones, A. J. Ryan, T. Gough, R. Vafabakhsh, and R. Golestanian, Self-Motile Colloidal Particles: From Directed Propulsion to Random Walk, Phys. Rev. Lett. **99**, 048102 (2007).
[45] K. Franke and H. Gruler, Galvanotaxis of human granulocytes: Electric field jump studies, Eur. Biophys. J. **18**, 334 (1990).
[46] V. M. Kadiri, C. Bussi, A. W. Holle, K. Son, H. Kwon, G. Schütz, M. G. Gutierrez, and P. Fischer, Biocompatible magnetic micro-and nanodevices: Fabrication of fept nanopropellers and cell transfection, Adv. Mater. **32**, 2001114 (2020).
[47] V. M. Kadiri, J.-P. Günther, S. N. Kottapalli, R. Goyal, F. Peter, M. Alarcón-Correa, K. Son, H.-N. Barad, M. Börsch, and P. Fischer, Light-and magnetically actuated fept microswimmers, Eur. Phys. J. E **44**, 74 (2021).
[48] D. Schamel, A. G. Mark, J. G. Gibbs, C. Miksch, K. I. Morozov, A. M. Leshansky, and P. Fischer, Nanopropellers and their actuation in complex viscoelastic media, ACS Nano **8**, 8794 (2014).
[49] D. Dasgupta, D. Pally, D. K. Saini, R. Bhat, and A. Ghosh, Nanomotors sense local physicochemical heterogeneities in tumor microenvironments, Angew. Chem., Int. Ed. **59**, 23690 (2020).
[50] S. Ghosh and A. Ghosh, Mobile nanotweezers for active colloidal manipulation, Sci. Rob. **3**, eaaq0076 (2018).
[51] G. Patil, E. Vashist, H. Kakoty, J. Behera, and A. Ghosh, Magnetic nanohelices swimming in an optical bowl, Appl. Phys. Lett. **119**, 012406 (2021).
[52] M. Pal, I. Fouxon, A. M. Leshansky, and A. Ghosh, Fluid flow induced by helical microswimmers in bulk and near walls, Phys. Rev. Res. **4**, 033069 (2022).
[53] D. Du, E. Hilou, and S. L. Biswal, Reconfigurable paramagnetic microswimmers: Brownian motion affects nonreciprocal actuation, Soft Matter **14**, 3463 (2018).

[54] P. L. Venugopalan, R. Sai, Y. Chandorkar, B. Basu, S. Shivashankar, and A. Ghosh, Conformal cytocompatible ferrite coatings facilitate the realization of a nanovoyager in human blood, Nano Lett. **14**, 1968 (2014).

[55] P. L. Venugopalan, S. Jain, S. Shivashankar, and A. Ghosh, Single coating of zinc ferrite renders magnetic nanomotors therapeutic and stable against agglomeration, Nanoscale **10**, 2327 (2018).

[56] R. Vasantha Ramachandran, R. Bhat, D. Kumar Saini, and A. Ghosh, Theragnostic nanomotors: Successes and upcoming challenges, Wiley Interdiscip. Rev. **13**, e1736 (2021).

[57] B. J. Nelson, I. K. Kaliakatsos, and J. J. Abbott, Microrobots for minimally invasive medicine, Annu. Rev. Biomed. Eng. **12**, 55 (2010).

[58] T. Qiu, M. Jeong, R. Goyal, V. M. Kadiri, J. Sachs, and P. Fischer, Magnetic micro-/nanopropellers for biomedicine, in *Field-Driven Micro and Nanorobots for Biology and Medicine* (Springer, New York, 2022), pp. 389–411.